

The middle Pleistocene transition as a generic bifurcation on a slow manifold

Peter Ashwin · Peter Ditlevsen

Received: 6 August 2014 / Accepted: 28 January 2015
© Springer-Verlag Berlin Heidelberg 2015

Abstract The Quaternary period has been characterised by a cyclical series of glaciations, which are attributed to the change in the insolation (incoming solar radiation) from changes in the Earth’s orbit around the Sun. The spectral power in the climate record is very different from that of the orbital forcing: prior to 1000 kyr before present most of the spectral power is in the 41 kyr band while since then the power has been in the 100 kyr band. The change defines the middle Pleistocene transition (MPT). The MPT does not indicate any noticeable difference in the orbital forcing. The climate response to the insolation is thus far from linear, and appears to be structurally different before and after the MPT. This paper presents a low order conceptual model for the oscillatory dynamics of the ice sheets in terms of a relaxation oscillator with multiple levels subject to the Milankovitch forcing. The model exhibits smooth transitions between three different climate states; an interglacial (i), a mild glacial (g) and a deep glacial (G) as proposed by Paillard (Nature 391:378–381, 1998). The model suggests a dynamical explanation in terms of the structure of a slow manifold for the observed allowed and “forbidden” transitions between the three climate states. With the model, the pacing of the climate oscillations by the astronomical forcing is through the mechanism of phase-resetting of relaxation oscillations in which the internal phase of the oscillation is affected by the forcing. In spite of its simplicity as a forced ODE, the model is able to reproduce not only

general features but also many of the details of oscillations observed in the climate record. A particular novelty is that it includes a slow drift in the form of the slow manifold that reproduces the observed dynamical change at the MPT. We explain this change in terms of a transcritical bifurcation in the fast dynamics on varying the slow variable; this bifurcation can induce a sudden change in periodicity and amplitude of the cycle and we suggest that this is associated with a branch of “canard oscillations” that appear for a small range of parameters. The model is remarkably robust at simulating the climate record before, during and after the MPT. Even though the conceptual model does not point to specific mechanisms, the physical implication is that the major reorganisation of the climate response to the orbital forcing does not necessarily imply that there was a big change in the environmental conditions.

Keywords Middle Pleistocene transition · Nonlinear oscillation · Ice age · Slow manifold · Bifurcation

1 Introduction

Climatic variations on multi-millennial time scales are recorded in deep-sea sediments. The enrichment of the ^{18}O isotope in the deposited foraminifera shells depends on ocean temperature and isotopic composition of the ocean water. The inventory of heavy isotope water in the ocean is a direct measure of the amount of preferentially light isotopes water stored in land based glaciers and ice sheets. The water temperature dependence of the biological isotope fractionation in the growth of the calcium carbonate shells makes the benthic foraminifera (bottom living) preferential as a global climate proxy rather than the planktonic foraminifera (living near the ocean surface), since the latter

P. Ashwin (✉)
Centre for Systems, Dynamics and Control, Harrison Building,
University of Exeter, Exeter EX4 4QF, UK
e-mail: P.Ashwin@exeter.ac.uk

P. Ditlevsen
Centre for Ice and Climate, Niels Bohr Institute, Juliane Maries
Vej 30, 2100 Copenhagen, Denmark

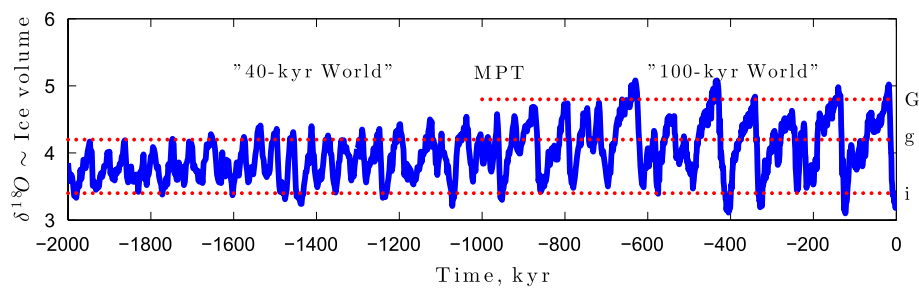


Fig. 1 The benthic foraminiferal oxygen isotope stack by Lisiecki and Raymo (2005) shows the middle Pleistocene transition from the “40-kyr World” of approximately 41 kyr oscillations between the interglacial (i) state and the mild glacial (g) state to the “100-kyr

World” of approximately 100 kyr oscillations; interglacial to mild glacial to deep glacial to interglacial (i → g → G → i), as proposed by Paillard (1998)

are more influenced by the local sea surface temperature (Shackleton et al. 2000). A stack of 57 globally distributed ocean sediment cores has been established as an account for the climate through the past 5.3 million years (Lisiecki and Raymo 2005). The dating of the sediment cores is a challenge, which is met by either assuming a linear relation with the orbital variations (orbital tuning) or by assuming constant sedimentation rates and an estimated compaction between dateable layers in the sediments (Huybers and Wunsch 2004; Huybers 2007). To avoid circular reasoning, the latter method is preferred when investigating the climatic response to the orbital changes.

Especially the summer insolation at high latitudes is thought to be the dominant component of the orbital forcing important for the waxing and waning of the Northern ice sheets. Consequently, the 65°N summer solstice insolation is termed the Milankovitch forcing (Berger 2012). The spectral power in the insolation is concentrated around the 23 kyr band from precession of the axis of rotation and around 41 kyr due to the obliquity cycle, which is the tilt of the rotational axis with respect to the ecliptic plane of Earth's orbit around the Sun. An order of magnitude weaker power occurs in the 100 and 400 kyr bands due to changes in the eccentricity of the orbit. The effect of changing eccentricity is mainly through modulation of the seasonal effect of precession (Hays et al. 1976); in a near circular orbit there is no difference between the distance to the Sun at summer and at winter, thus the precession has no influence on the total insolation.

The paleoclimate record (Fig. 1) shows that the climatic response to the orbital forcing changed dramatically around 1000 kyr BP and various authors have studied aspects of, and possible reasons for, this change (Mudelsee and Schulz 1997; Huybers 2009; Meyers and Hinnov 2010; Imbrie et al. 2011; McClymont et al. 2013; Daruka and Ditlevsen 2014). Prior to the change, denoted as the middle Pleistocene transition (MPT), the glacial cycles lasted approximately 40 kyr (the “40 kyr world”), while after the

MPT the glacial periods became colder and lasted approximately 100 kyr (the “100 kyr world”). Here we shall define the MPT to occur at 1000 kyr BP, even though it is not a sharp transition (Clark et al. 2006); we note that a detailed analysis of the changes of forcing and responses over this period has been undertaken by Meyers and Hinnov (2010) and Rial et al. (2013). The 100 kyr world is characterised by an asymmetry with respect to time reversal, which is not present in the insolation. The transitions into the glacial state (the inceptions) are gradual, corresponding to a slow buildup of ice sheets. By contrast the transitions into the interglacial states (the terminations) are much more rapid, corresponding to a breakdown of ice sheets within a few millennia or even shorter. Unfortunately, the dating uncertainty in the climate record is of the order of thousands of years (Lisiecki and Raymo 2005; Hilgen et al. 2012; Huybers and Wunsch 2004), which is on the order of a quarter period of the precession cycle. Thus the limited accuracy prevents us from directly attributing the terminations, except from the last termination, to a specific component and phase of the orbital forcing, see also Imbrie et al. (2011). The last termination is well dated from ice core records (North GRIP members 2004), which also have a much better temporal resolution than the ocean sediment cores. The $\delta^{18}O$ isotope records from ice cores are proxies for atmospheric temperatures, ice being more depleted of ^{18}O water when it is cold. The ocean sediment $\delta^{18}O$ is consequently thought to be a proxy for total ice volume (Sima et al. 2006).

The issue of which component of the insolation forcing correlates best with the climate response (De Saedeleer et al. 2013) is not our concern here. In the rest of the paper, we shall simply assume the 65N summer solstice insolation (Milankovitch forcing) to be the relevant forcing.

1.1 Spectral characteristics

The uncertainty in the phasing between the forcing and the response is not only due to dating uncertainty, it also

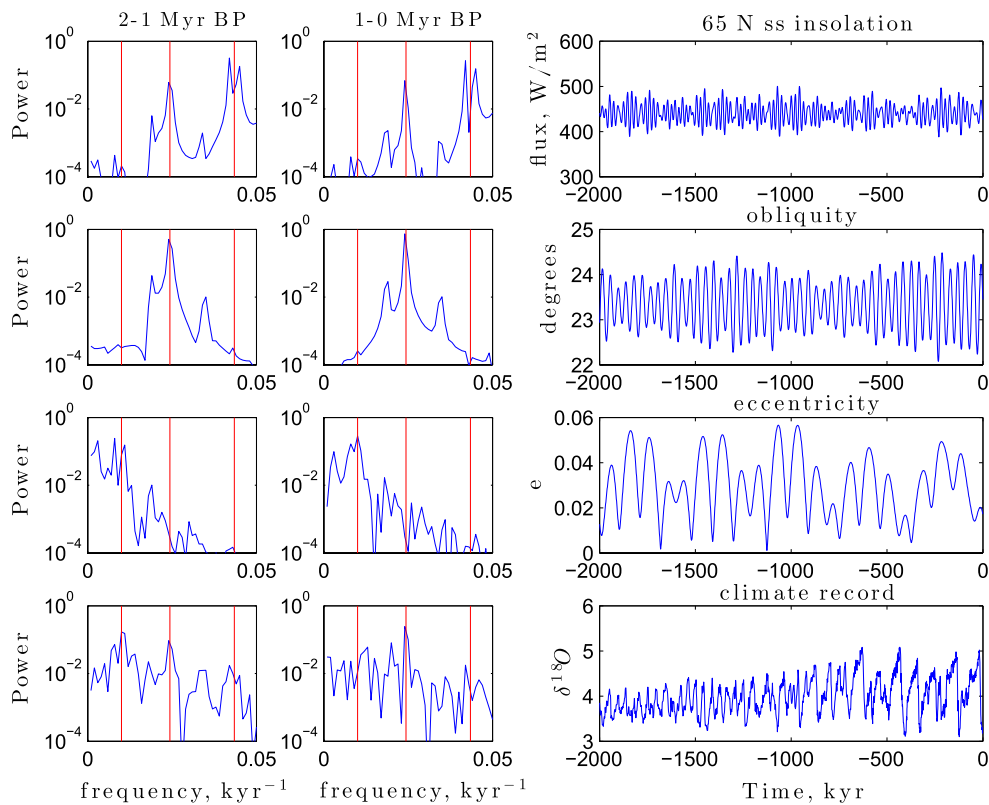


Fig. 2 Power spectra (*left column* before MPT and *middle column* after MPT) and timeseries (*right column*). Milankovich forcing (*top row*), obliquity and eccentricity signals only (*middle rows*) and climate record (*bottom row*). Even with unknown response times and

phases, if the response was linear then the spectral power in the climate response should be similar to the spectral power in the forcing before and after the MPT

reflects our limited understanding of the response times in the climate system. Thus for now we ignore the phases and compare the spectral power between the forcing and response curves directly. For that we will concentrate on the last two million years, comparing the two periods (a) 2000–1000 kyr BP, prior to the MPT and 1000–0 kyr BP posterior to the MPT. Taking the forcing to be the 65°N summer solstice insolation, this is dominated by the precession cycle around 23 kyr and with some weight on the obliquity cycle at 41 kyr and virtually no weight in the 100 kyr band. As is seen in Fig. 2 top panels, there is very little difference between the periods 2000–1000 kyr BP and 1000–0 kyr BP. Contrary to that, the climate response changes from 41 kyr to around 100 kyr at the MPT, as seen in the bottom panels; see also the analyses of Meyers and Hinnov (2010) and Rial et al. (2013). Note that there is power at the 41 kyr band also after the MPT.

1.2 Glacial cycles in climate models

Current numerical climate models are not capable of simulating glacial cycles, led alone the MPT, based solely on the changing insolation (first-principle models). The 100 kyr

world has recently been simulated in an extensive ice sheet model, forced by output from a GCM, run in time slice experiments with changing insolation and ice sheet configurations (Abe-Ouchi et al. 2013). In that paper it is demonstrated that the 100 kyr cycle does not rely on the eccentricity component of the forcing and the cyclicity comes from a hysteresis in the mass balance of the North American Laurentide ice sheet. Their model was fed with and without the observed 100 kyr variation in the atmospheric CO_2 from the interchange with the oceans. With a constant level of 220 ppm, and solely forcing by obliquity, their model shows the 41 kyr periodicity.

Several suggestions have been made for the physical mechanisms governing glacial dynamics. A comprehensive review of suggested mechanisms can be found in Crucifix (2012). In low dimensional models the dynamics are reduced to a few degrees of freedom in order to explain the behaviour. Here we shall list a few: In Maasch and Saltzman (1990) an oscillator model is proposed: Ice masses depending on insolation and greenhouse warming, atmospheric CO_2 concentration depending on ocean temperature and state of the ocean depending on the ice masses. In Tziperman and Gildor (2003) a sea-ice switch mechanism is proposed: this is also

an oscillator model, where growing ice sheets leads to lower temperatures and advancing sea-ice cover, which in turn leads to decreased precipitation over the ice sheets leading to ice sheet retreat. The dynamical explanation of the MPT is different between the different models. In the first model, the MPT is due to a Hopf-bifurcation as a result of change in some model parameter, which is speculated to be due to tectonic changes, such as the raise of the Tibetan Plateau. For this model the 41 kyr world prior to the MPT is thus not a self-oscillation, but a linear response to the obliquity cycle. The sea-ice switch mechanism involves a structural changing threshold for sea ice formation depending on deep ocean temperature. In the latter model the deep sea temperature is the control parameter leading to a Hopf-bifurcation at the MPT. Alternatively, it was proposed that ice sheet stability depends on bottom sliding, such that long term reolith erosion by the North American ice sheets let to possibility of larger stable ice sheets after the MPT (Clark and Pollard 1998).

The climate system is obviously extremely high dimensional and complex, which might question the relevance of reduced models of only a few degrees of freedom. However, it seems that despite distinct regional variations, climate records across the globe are quite synchronous and robust, as observed in sediment cores from all ocean basins, ice cores from both poles, speleotherm and coral records. This suggests that the climatic response to the orbital forcing can be, to a good approximation, captured by a single time series. Note also that even though the insolation field varies strongly with latitude and time of year, the field depends on a low number of orbital parameters. Thus, the dynamics governing the climate record could indeed be captured by a few dominant variables with any further variability described by a noise term. In terms of the forcing-response in the glacial cycles, different dynamical mechanisms have been proposed. These can roughly be categorised as either self-sustained non-linear oscillators (Källen et al. 1979; Saltzman and Sutera 1987), forced nonlinear oscillators (LeTreut and Ghil 1983) or non-oscillating, but responding to the oscillatory forcing, such as stochastic (Benzi et al. 1982; Ditlevsen 2009) or coherence resonance (Pelletier 2003).

Here we shall focus on a possible dynamical explanation for the glacial cycles and the mechanism behind the MPT, thus we propose a new conceptual dynamical model of Pleistocene ice dynamics that, in the absence of variation in insolation, displays relaxation oscillations between glacial and interglacial states both before and after the MPT [which agrees with a conclusion of Ashkenazy and Tziperman (2004)]. As such we combine a number of elements used in relaxation models of the Pleistocene ice ages (Crucifix 2012) while making assumptions that give a generic form of model.

The paper is organized as follows. In Sect. 2 we introduce a class of conceptual models where the main observable (ice volume) is forced by insolation and relaxes towards a value

that depends on the “climate state”. The latter state is modelled by a second equation that admits possible multiple states with hysteresis over a short timescale. On slowly varying a parameter that changes the number of “climate states” from two (before the MPT) to three (after the MPT) in a generic manner, we arrive at our model for the MPT. Our model is a continuous dynamical ODE model inspired by the rule based switch model proposed by Paillard (1998), we thus identify a robust generic dynamical origin for the switch model: Prior to the MPT the 41 kyr cycles oscillator between two equilibrium states, a mild glacial g and an interglacial i state. At the MPT a third deep glacial state G becomes accessible due to the cooling, such that the glacial cycle becomes $i \rightarrow g \rightarrow G \rightarrow i$. Section 2.2 describes the oscillation mechanisms before and after the MPT and demonstrates that the transition corresponds in a certain sense to a transcritical bifurcation on the slow manifold. Under the addition of astronomical forcing, in Sect. 3 we show that this deterministic model can produce remarkable agreement with the ocean sediment climate record of Lisiecki and Raymo (2005); we compare the model for no forcing as well as for Milankovitch and for purely periodic forcing. Finally, Sect. 4 discusses some of the challenges to finding a physical justification to the climate state variable as well as connections to other work on forced oscillations.

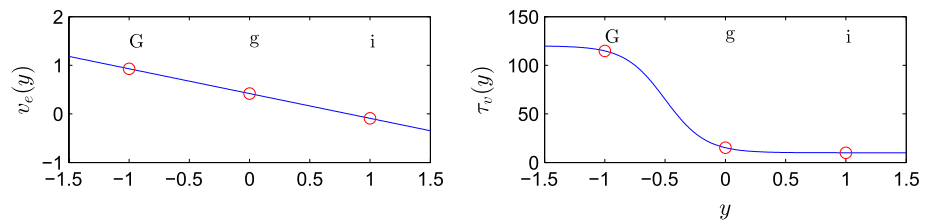
2 The model: relaxation oscillations under astronomical forcing

As climate models based on first principles also seem to exhibit different states as a consequence of the non-linear response to the insolation, a different approach is to assume multiple equilibrium states (Paillard 1998). Based on the observed record we aim to find an effective (minimal) low dimensional dynamics which describes the glaciations and shows the structural change causing the MPT. We take this observed record as our target for the global ice volume variable $v(t)$ as a function of time. This variable is coupled to an (unobserved) climate-state variable $y(t)$. The most general model we consider here is:

$$\begin{aligned} \frac{dv}{dt} &= \frac{v_e(y) - v}{\tau_v(y)} - \frac{I(t)}{\kappa_f} + \sigma_v \eta_v \\ \frac{dy}{dt} &= H(y, v, \lambda(t)) + \sigma_y \eta_y \end{aligned} \quad (1)$$

where the ice volume v (the observable) depends the climate state variable y . The quantities $\sigma_{y,v}$ are noise amplitudes for the additive noise $\eta_{y,v}$ though we will mostly consider the case $\sigma_y = \sigma_v = 0$. The v response is similar to that of Paillard (1998): We assume the ice volume to relax to an equilibrium state $v_e(y)$ with a relaxation timescale $\tau_v(y)$, both depending on the climate state y , but independent from the insolation. The forcing related to the summer melt-off is

Fig. 3 The equilibrium state for ice volume and the relaxation time as functions of the climate state



governed by the astronomical (Milankovitch) variation of the insolation $I(t)$. The reaction time scale κ_f can be interpreted as being associated to a heat capacity of the ice sheets.

For the y dynamics, the drift function $H(y, v, \lambda)$ describes a nonlinear relationship between the climate state y and the ice volume v such that multiple equilibrium solutions for y of $H(y, v, \lambda) = 0$ may be possible for a range of values of v and λ . The variable λ represents a structural parameter that will slowly change over the course of the Pleistocene.

The nonlinear relationship H is chosen (see “Appendix”) to reflect the Paillard interpretation of the observed record, so that we can identify

$y \approx$	state	name
1	interglacial	i
0	minor glacial	g
-1	major glacial	G

(2)

We will assume the equilibrium state of v depends on y simply as a linear function of the climate state (Fig. 3, top panel)

$$v_e(y) = \beta(\alpha - y). \quad (3)$$

For increasing y we expect less ice in the equilibrium state and so $\beta > 0$ and $\alpha > 0$ will be assumed; the default choice for these will be $\alpha = 0.82$ and $\beta = 0.51$.

The state-dependent timescale $\tau_v(y)$ for v is assumed to be different in the different climate states; in the i state the ablation of ice will occur at a different timescale to that of ice growth in the G state. To this end we choose a smooth function (Fig. 3, bottom panel)

$$\tau_v(y) = \frac{1}{2} [(\tau_i - \tau_G) \tanh(\mu(y - y_p)) + \tau_G] \quad (4)$$

that gives $\tau_v(y) \approx \tau_G$ (for $y \approx -1$) and $\tau_v(y) \approx \tau_i$ (for $y \approx 1$), where τ_i, τ_G are constants and the constants y_p and $\mu > 0$ governs how fast the rates changes with y . In what follows, we will choose the constants: $\tau_i = 20$, $\tau_G = 130$, $\mu = 3$ and $y_p = -0.5$.

2.1 Fast–slow dynamics and the slow manifold

The model (2) can be viewed as a fast–slow system where the climate state y (fast variable) quickly approaches a quasi-equilibrium state while the ice volume v (slow

variable) evolves on a slower timescale. Because of this we expect the y dynamics to be quickly attracted to a neighbourhood of a solution of the slow manifold, where the latter is described implicitly by the zero set

$$H(y, v, \lambda) = 0. \quad (5)$$

The assumption of multiple climate states means we need to find a suitable H with multiple solutions $y(v, \lambda)$ to (5) for a range of v and λ . The y dynamics can be used to determine whether a solution on the slow manifold is stable (attracting for y) or unstable (repelling for y) and divides the slow manifold into a union of stable and unstable sheets and solutions will spend longer time closer to this slow manifold as the timescales become more highly separated.

A solution of (2) will explore a stable sheet of the slow manifold most of the time, except when it encounters a fold—namely, where stable and unstable sheets meet on varying v and λ . As the solution hits a fold, it will “fall off” the slow manifold and move to a different sheet. This mechanism allows a transition from one climate state to another occurring at folds of the surface (5), i.e. tangents to v constant.

Although we are assuming a timescale separation, the model will evolve on a number of possible timescales— y will vary the fastest (assumed to be associated with ocean–atmosphere circulation patterns) while v will vary at a slow rate according to which of the various $i/g/G$ states are indicated by y . Finally, the slow secular variation of λ will vary on an even longer timescale.

By considering the transitions we need over the MPT we can choose a slow manifold $H(y, v, \lambda)$ as detailed in “Appendix” and illustrated in Fig. 4. This choice gives transitions according to the selection-rules proposed by Paillard; namely

- Before the MPT we have transitions from i to g on decay of v and from g back to i on growth of v .
- After the MPT we have transitions from i to g on decay of v , from g to G and them from G back to i on growth of v .
- We discuss this choice of H in the final section.

2.2 Dynamics and bifurcation for static λ

For fixed λ and in the absence of noise or astronomical forcing, cross sections of the slow manifold (5) give the slow manifold for evolution of the system in the (y, v) plane. If

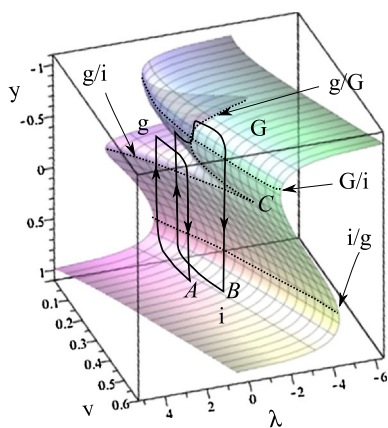


Fig. 4 The slow dynamics is assumed to take place close to this surface defined by $H(y, v, \lambda) = 0$, with H defined by (11, 12) in “Appendix”. There are *three sheets* of the surface that are attracting—these are labeled i, g and G and correspond to stable climate regimes. The attracting regions are bounded by folds indicated by *dashed lines*; at these folds the fast dynamics transits to another attracting region as indicated. For slow ramping of λ the dynamics on the slow manifold is such that there is a transition from cycles of the form A between i and g states to cycles of the form B that visit i, g and G states. There is a large-scale hysteresis between G and i states for a range of forcing λ and v . The cusp C gives the third g state for small values of v and λ .

λ changes slowly with time then the dynamics undergoes drifting relaxation oscillations, where y jumps between a number of stable branches corresponding to $i/g/G$ states. Figure 5 illustrates the dynamics for the model on varying λ : observe that for $\lambda \leq 0$ (left panel) the oscillations go around the loop $i \rightarrow g \rightarrow G \rightarrow i$ while for $\lambda > 0$ (right panel) they go around the loop $i \rightarrow g \rightarrow i$. The middle panel shows the transition, namely a transcritical bifurcation of the slow manifold in the fast dynamics.

We can view this transition as a generic bifurcation of the one-dimensional dynamics for $\frac{dy}{dt} = H(y, v, \lambda)$ on varying v at $\lambda = 0$; note that by solving $H_y = H_v = 0$ we have $(v, y) = (0.297, -0.237)$ and substituting this into $H = 0$ we find $\lambda = 0$. Although the only generic codimension one bifurcations of equilibria in this system is the saddle-node (also called the fold or limit point bifurcation) (Kuznetsov 2004) and the only generic codimension two bifurcation is the cusp. However, this approach views all parameters as equal—and indeed, one can view the transition in Fig. 5 middle panel as simply an exceptional path through a line of saddle-node bifurcations in the (v, λ) -space that is tangent to the line $\lambda = 0$. It is useful to view this as a bifurcation problem with v as a “distinguished parameter” (Golubitsky and Schaeffer 1985). This means that we are interested in how the bifurcation diagram of y versus v changes as we change further parameters; in this case λ ; this is appropriate here as there is an assumed timescale separation between the slow variable v and the very slow λ . Using this approach we can see that the bifurcation at $\lambda = 0$ is indeed a generic transition of transcritical type between a case where there are to saddle-nodes and a case where there are none; in nondimensionalised variables Y and v local to the bifurcation at $(Y, V) = (0, 0)$ and μ near $\lambda = 0$ for

$$\dot{Y} = F(Y, V, \lambda) \tag{6}$$

then we claim the bifurcation of the equilibrium $F(0, 0, 0) = 0$ can be modelled by assuming $F_Y(0, 0, 0) = F_V(0, 0, 0) = 0$ and otherwise generic choice of Taylor series at $(0, 0, 0)$. Let us define $a = F_{YY}(0, 0, 0), b = F_{VY}(0, 0, 0), c = F_{VV}(0, 0, 0)$ and $d = F_\lambda(0, 0, 0)$. Then we can write the Taylor series of the bifurcation problem as

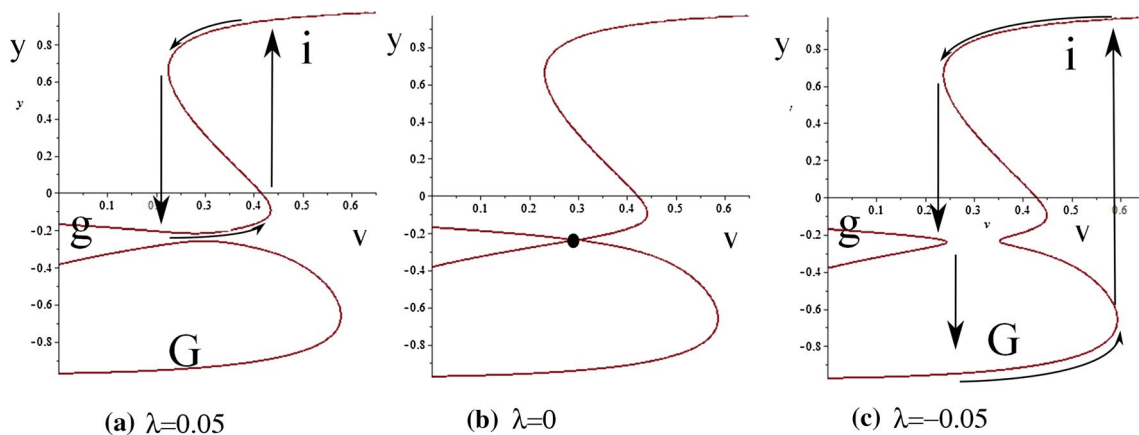


Fig. 5 The *red curves* show the manifold in the (v, y) -plane on decreasing λ . The dynamics moves between interglacial i , mild glacial g and deep glacial G states and the *arrows* indicate the time evolution via the slow (*small arrow*) and fast (*large arrow*) dynam-

ics. Observe that the transcritical bifurcation of the slow manifold at $\lambda = 0$ causes the relaxation oscillations to abruptly change amplitude (and period). **a** $\lambda = 0.05$, **b** $\lambda = 0$, **c** $\lambda = -0.05$

Fig. 6 (Left) period and (right) maximum v on the attracting cycle for the unforced system [$I(t) = 0$] on varying λ ; note the very rapid change in period near $\lambda = 0$ associated with the bifurcation in the slow manifold shown in Fig. 5. The branch of periodic solutions changes over a small range of λ

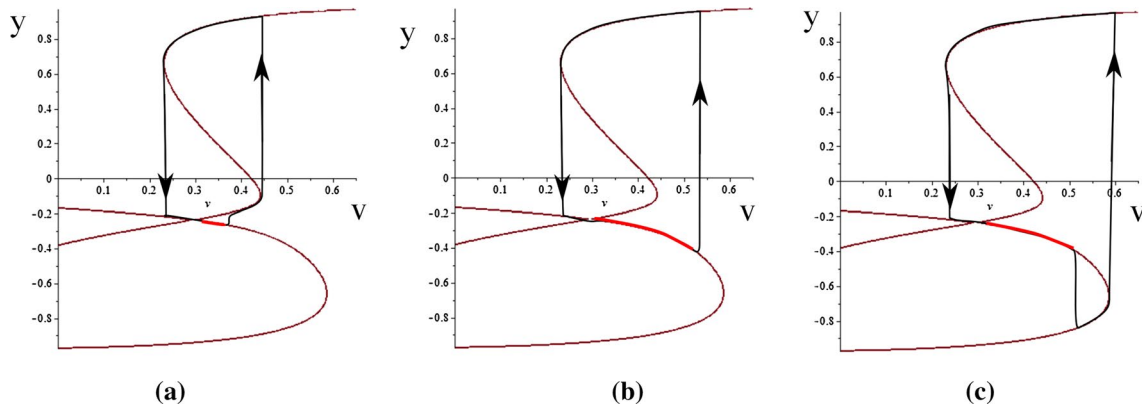
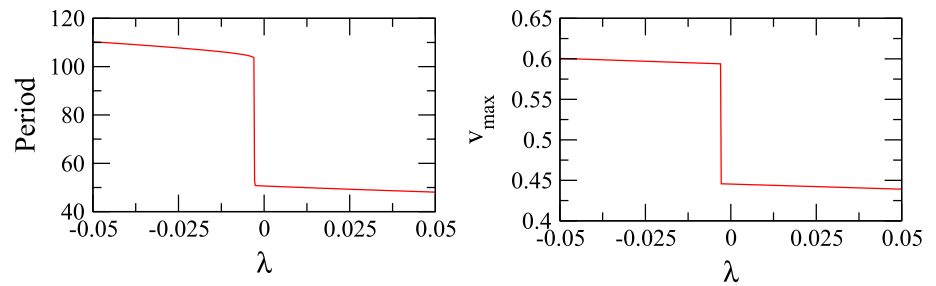


Fig. 7 Near the transcritical bifurcation of the slow manifold at $\lambda = 0$ shown in Fig. 5, between the oscillations (a, c) in that figure there will be a sequence of periodic orbits with “canard” trajectories

as shown in the sequence (a–c) here. Note that these are topologically different oscillations, each of which includes a segment (highlighted in red) that is close to an unstable part of the slow manifold

$$\dot{Y} = aY^2 + bYV + cV^2 + d\lambda + \text{higher order terms} \quad (7)$$

As long as the quadratic form $aY^2 + bYV + cV^2$ is non-degenerate and of indeterminate type (i.e. $b^2 - 4ac > 0$) then higher order terms will not affect the branching near $(0, 0, 0)$ and the bifurcation will be of transcritical type. Given that we have imposed two constraints on the equilibrium, this means that the bifurcation of this type is a generic codimension two bifurcation for the distinguished parameter system (7). The global dynamics near this transition will be very interesting in that the branch of stable periodic solutions that connects the smaller to the larger oscillations; Fig. 6 shows the change in period of the attracting cycle on passing through the transition, treating λ as a bifurcation parameter.

The transition in periodic orbits shown in Fig. 6 will include a range of canard trajectories that traverse sections of the unstable section of the slow manifold—the transition is a type of “canard explosion” (Krupa and Szmolyan 2001) but one that connects two large amplitude stable oscillations; consideration of vector fields on the branch of solutions means that it must go through intermediate oscillations with a variety of different canard trajectories, as shown in Fig. 7.

3 The MPT with or without astronomical pacing

We now return to the full model (2) under the assumption that $\lambda(t)$ shows a secular variation with time and forcing and in the absence of noise. More precisely we assume

$$\lambda(t) = \lambda_0 + \lambda_1 t, \quad \lambda_0 = -0.10553, \quad \lambda_1 = -10^{-4} \text{ kyr}^{-1} \quad (8)$$

(units for t is kyr and is measured such that $t = 0$ is present). This means that $\lambda = 0$ at approximately 1000 kyr BP). Figure 8 shows the evolution of the model with (8) show in (b) and no forcing, $I = 0$ for randomly chosen initial conditions at time 2,500 kyr BP, projected onto various axes. Observe in (d) the transition from small amplitude oscillations of v with approximately 41 kyr period to larger amplitude oscillations with approximately 100 kyr period around the 1000 kyr BP. This corresponds in (a) to a change from relaxation oscillations that go around the upper square to relaxation oscillations that visit all three levels. The remaining panels (c) show the oscillations in terms of the y variable while (d,e) show the instantaneous values of $v_e(y)$ and $\tau_v(y)$ in (2).

For astronomical forcing we use a Fourier representation along the lines of Berger (1978) of the defect of summer

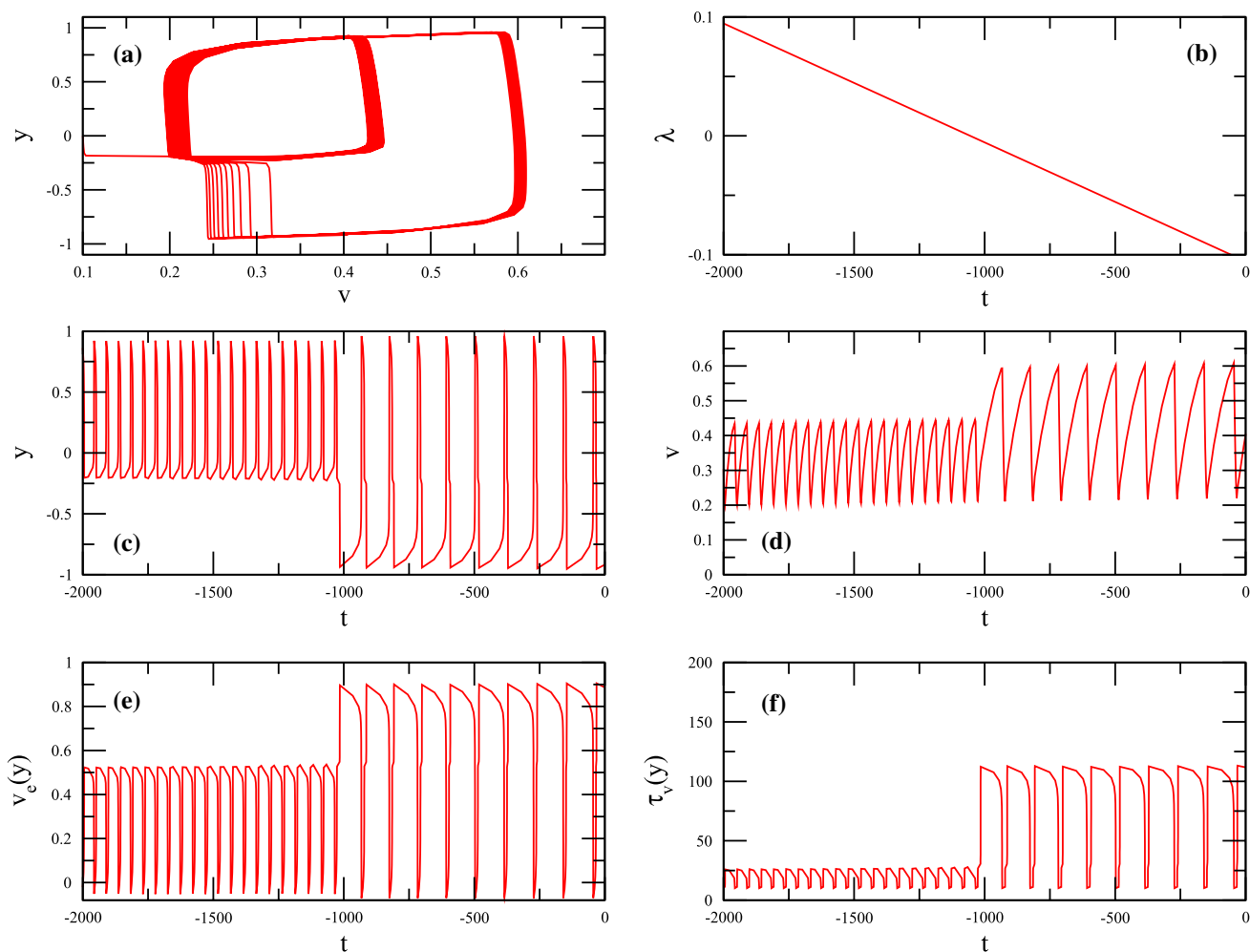


Fig. 8 **a** v against y for the system without astronomical forcing [$I(t) = 0$] but with **b** prescribed drift (8) of λ that takes the system through the transcritical bifurcation on the slow manifold at approx $t = 1000$ kyr before present. **c–f** Timeseries of the quantities y, v, v_e

and τ_v for the trajectory in **a**. Observe the fluctuations in $y, v_e(y)$ and $\tau_v(y)$ as the system changes between G, g and i states, while the ice volume proxy v accumulates information about the state y

solstice insolation at 65°N from its mean values, as given in De Saedeleer et al. (2013), namely

$$I(t) = \sum_{k=1}^{35} [s_k \sin(\omega_k t) + c_k \cos(\omega_k t)] \tag{9}$$

and the values of the mode s_i, c_i, ω_i listed in (De Saedeleer et al. 2013, Appendix 1). Although this is designed to be an optimal fit in the time period from 1000 to 0 kyr BP, when compared to the more detailed model of Laskar et al. (2004) it fits well for the whole of the period 2000–0 kyr BP. Figure 9 shows the dynamics of the model (2) using (8, 9) to specify $\lambda(t), I(t)$ and choosing the following remaining parameters:

$$\kappa_f = 2,500, \quad \sigma_y = \sigma_v = 0. \tag{10}$$

To better understand the influence of the astronomical forcing, Fig. 10 shows runs of the model (2) for slowly ramped $\lambda(t)$ (8) under different forcing. The top panel reproduces the second panel of Fig. 9 (i.e. astronomical forcing (9), no noise) for convenience of comparison. The second panel shows the case for no noise and no forcing $I = 0$, while the third adds white noise to the v dynamics with $\sigma_v = 0.01$. Finally, the bottom panel shows the response for a pure harmonic forcing $I(t) = \sin(\Omega t)$ with $\Omega = 2\pi/41$ (solid line) and $I(t) = 20 \sin(\Omega t)$ with $\Omega = 2\pi/23$ (dashed line). Observe that the astronomical forcing noise free case appears to be able to best reproduce the observed fluctuations compared to any of the other cases. For the periodic forcing observe that phase locking appears both before and after the MPT for most of the response periods.

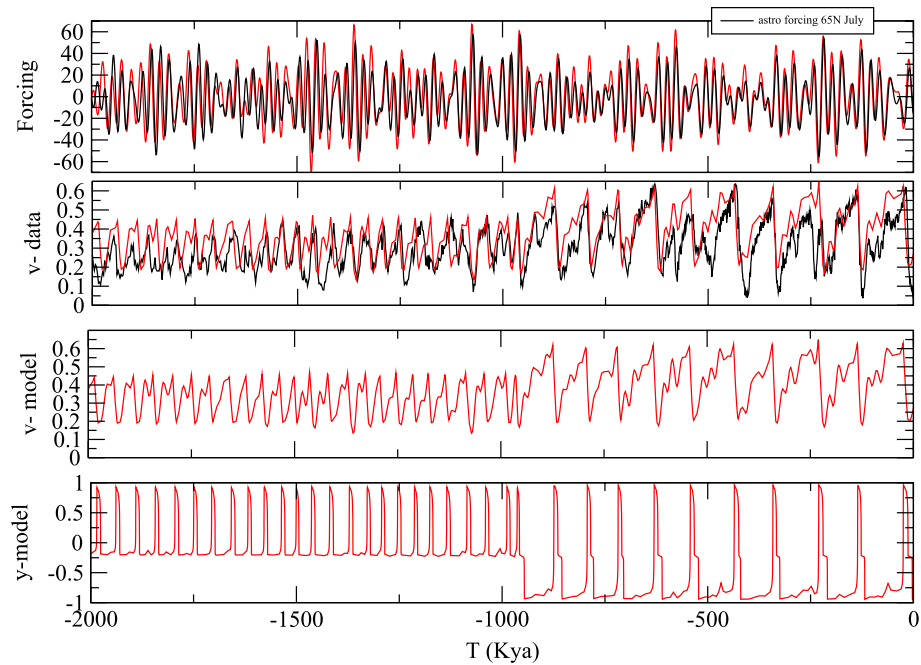


Fig. 9 Astronomically forced oscillations; the *top panel* shows (black) the astronomical forcing as summer peak insolation at 65°N from Laskar et al. (2004) and (red) the approximation (9) from De Saedeleer et al. (2013). The *second panel* shows (black) the climate record (Lisiecki and Raymo 2005) from the ocean sediment cores linearly scaled to fit the range of v from the model, along with (red) showing the model output from (2) using (8, 9). Observe a good qualitative agreement between model and record both before and after the

MPT at around 1000 kyr BP. The *final two panels* show the model output in v and y respectively; before the MPT the oscillation of y between 0 and 1 corresponds to a relaxation oscillation between i and g states; after the MPT the oscillation reaches i, g and G states. The forcing not only adds a modulation onto the v dynamics, but also moves the positions of the transitions relative to the unforced case, see e.g. Fig. 8

Fig. 10 From top to bottom: **a** model with astronomical forcing and no noise (red) together with climate record (Lisiecki and Raymo 2005) (black), **b** no astronomical forcing ($\kappa_f = \infty$) and no noise, **c** no astronomical forcing and added noise $\sigma_v = 0.01$, **d** astronomical forcing replaced with pure periodic sinusoidal forcing at period 41 kyr (solid line) and 23 kyr (dashed line)

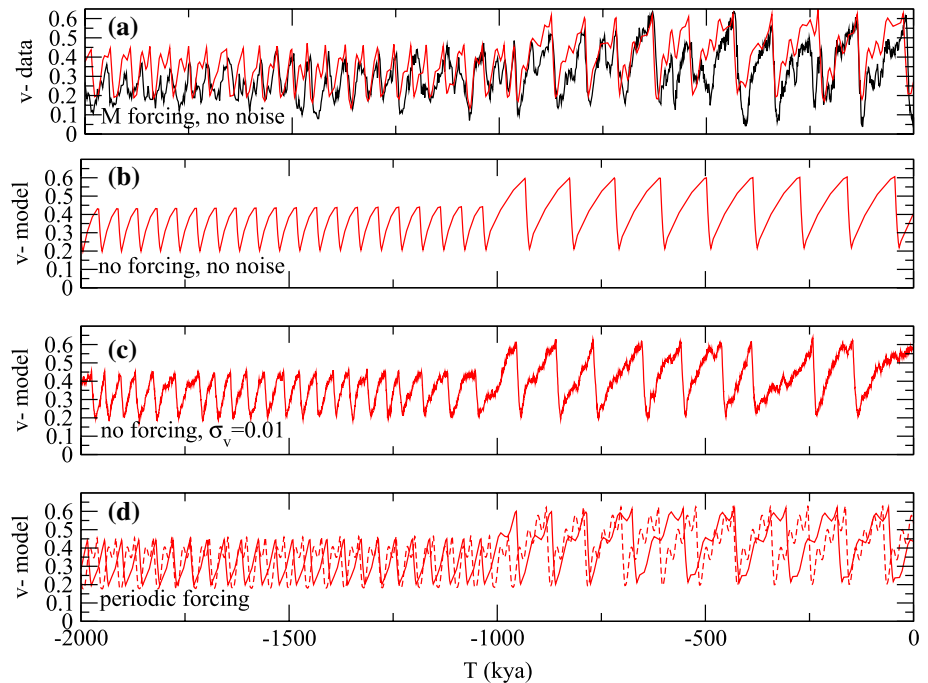


Fig. 11 From top to bottom: **a** astronomical forcing, **b** climate record (Lisiecki and Raymo 2005) compared to model output for two cases; *solid red* as in Fig. 9 and $\lambda_1 = -10^{-4}$, *dashed blue* using more rapid ramping of $\lambda_1 = -10^{-3}$, $\tau_g = 100$ and $\kappa_f = 1,900$. Observe the transition to large amplitude cycles in both case, and similar features before and after the transition

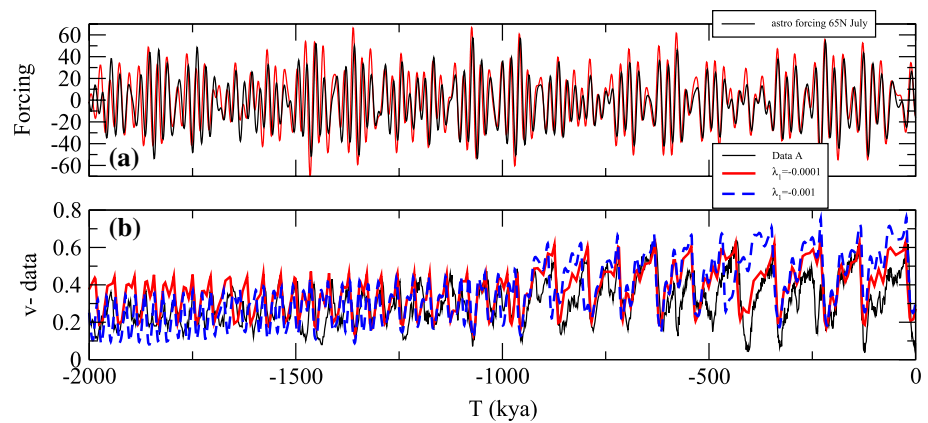
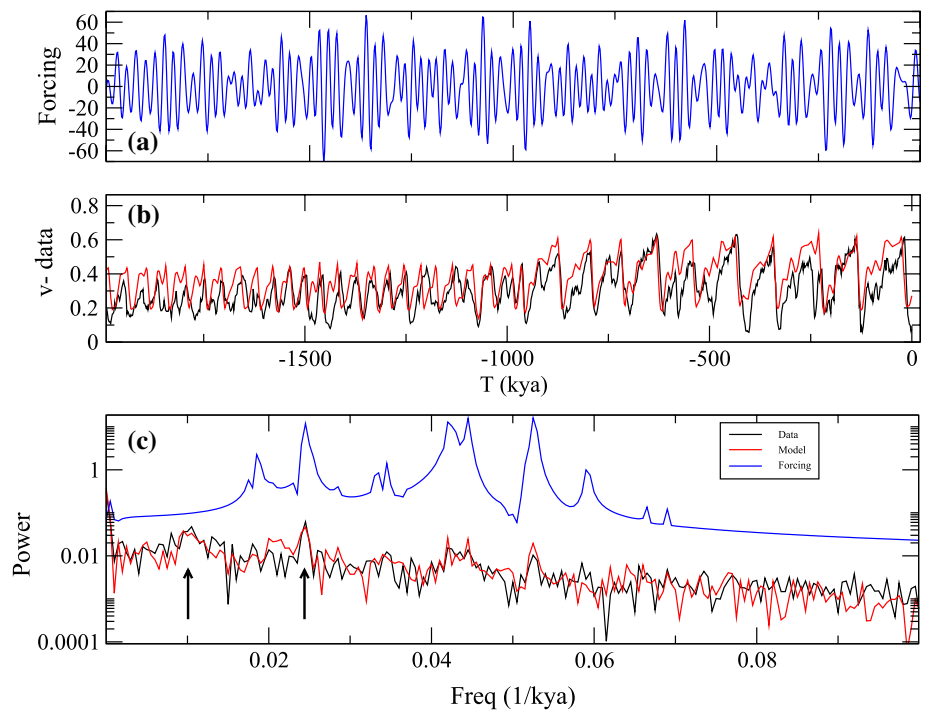


Fig. 12 From top to bottom: **a** astronomical forcing, **b** climate record for compared to model output (*red*) compared to Lisiecki and Raymo (2005) as in Fig. 9, **c** power spectra of the signals shown in **a**, **b**. Observe the good spectral agreement of the model, including the peaks denoted by *arrows* corresponding to periods 100 and 40 kyr. Only the latter peak is identifiable in the forcing. The spectrum of the forcing is vertically displaced because the signal is in different units



We note that the changing the rate of variation of λ does not appear to have a major influence; Fig. 11 illustrates the output of the model for two cases of λ_1 varied by a factor of 10. Some minor adjustment of the parameters κ_f and τ_g allow one to recover qualitatively similar results, details can presumably be recovered by careful optimization of parameters for the more rapid variation of λ .

Finally, we return to the question of the frequencies present in the forcing, the data and model response to the forcing. Figure 12 clearly shows that over the past 2000 kyr the model and data agree well in terms of spectral power. There are identifiable peaks in the response at the peaks of the forcing frequency while there is also an identifiable peak at frequency 0.01 corresponding to 100 kyr period that is not present in the forcing. These spectra were calculated by

interpolating the data and signal to a 2 kyr grid and then performing a Discrete Fourier Transform of the signal over the whole 2000 kyr.

4 Discussion

We have presented a new pure-ODE model that is able to do a reasonable job of modelling the climatic fluctuations over the past 2000 kyr. It is based on astronomical forcing of a relaxation oscillator, with states similar to those in Paillard (1998), that undergoes a transcritical bifurcation on the slow manifold at the MPT. In particular, we have an alternative explanation of the MPT in terms of bifurcation theory—rather than being a Hopf bifurcation (Maasch

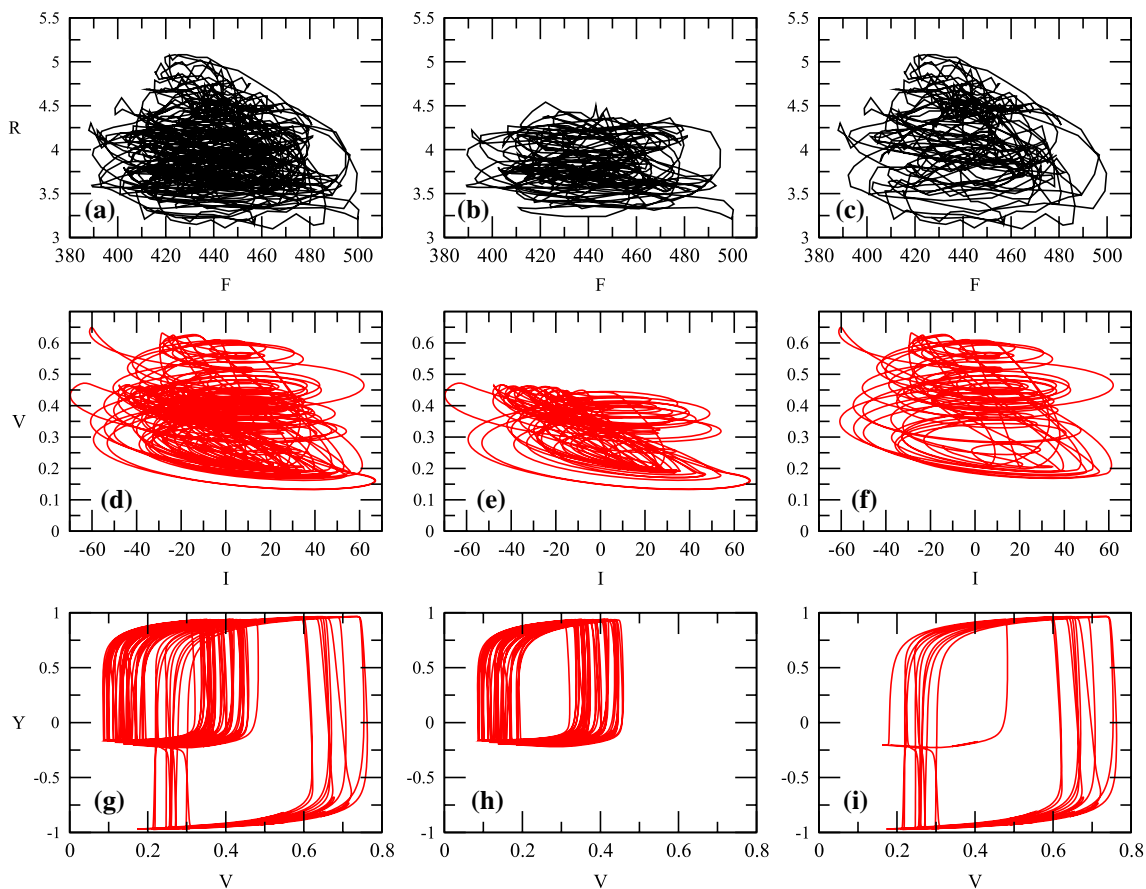


Fig. 13 Comparison of astronomical forcing and response for data and model. **a–c** Climate record $R(t)$ plotted against Milankovitch forcing $F(t)$. **d–f** Ice volume $V(t)$ plotted against the astronomical forcing anomaly $I(t)$. Observe a striking lack of simple correlation,

though the early Pleistocene (**b, e**) and the late Pleistocene Epochs clearly show the shift to larger amplitude for data and model. **g–i** Model dynamics plotted as $Y(t)$ against $V(t)$ where the slow manifold structure becomes visible

and Saltzman 1990) our model has a natural frequency of oscillation both before and after the MPT, but this changes abruptly due to a bifurcation in the structure of the slow manifold. The model combines features of a number of models reviewed in Crucifix (2012) while proposing a new generic candidate mechanism for the dynamical transition underlying the MPT. Indeed, the analysis of the strong asymmetry of the ice ages before the MPT by Ashkenazy and Tziperman (2004) suggests that these oscillations are nonlinear, self-sustained and approximately locked to the 41 kyr forcing. Our study gives a scenario how such oscillations may undergo an abrupt change in frequency and amplitude, even when the changes to model parameters are small and slow.

We have shown that the “bifurcation on a slow manifold” mechanism for the MPT can be thought of as a type of “canard explosion” (Krupa and Szmolyan 2001), though apparently not of a type that has been investigated in the literature; compare for example (Benoît et al. 1981; Wechselberger 2012). Nonetheless, the implication of the

model is that the transition occurs over a very short interval in parameter space, and hence the intermediate states would not necessarily be observable in the climate record; Fig. 13 compares the response of the climate system and of the model to astronomical forcing both before and after the MPT.

The relaxation oscillations of the unforced model before and after the MPT are of longer period than observed under astronomical forcing, but we suggest that this may not be a coincidence. We suggest that the relaxation oscillations may be accelerated by forcing in a similar way that a human circadian pacemaker, the Supra-chiasmatic nucleus (SCN) has a natural period that is slightly longer than 24 h, but is entrained by diurnal forcing on a 24 h period (Golombek and Rosenstein 2010); this can be observed in Fig. 10 where forcing with period 41 or 23 kyr apparently leads to a shortening of period of the oscillations; this is the case if the “phase response curve” (that determines how forcing affects the oscillation phase) predominantly advances the phase in the presence of forcing.

One possible criticism is that the functional form of the slow manifold (11) is somewhat contrived, however we note:

- (a) Only the topology of the level set (5) and the sign of H are actually important for the detailed dynamics; the time spent anywhere away from the level set is very small and determined by fast switched in the value of y .
- (b) The topology of this level set is generic (i.e. all singularities are robust to perturbations) and suggested by the multiple $i/g/G$ climate states of Paillard (1998).
- (c) We believe that other quite different constructions of H that give the same topological features will give models that are just as good, if not better, models for the climate record; in this sense the model is quite general.

On the point (c), we remark that for example the inclusion of possibly a large number of fast variables need not necessarily change the conclusions of the model, as long as these fast variables are effectively slaved to the modelled variables.

We have left the interpretation of the slow drift $\lambda(t)$ open; this could be due to minor and long term variation in solar output, by gradual weathering of land surface affected by ice, or for example tectonic changes as suggested in the introduction. It would be helpful to interpret the climate states y in terms of physical configurations such as mean flow patterns in atmosphere and ocean, features in the cryosphere or evolutionary developments, though the descriptive and predictive power of the model and the associated transition do not depend on this. The nature of the bifurcation shown in Fig. 6 is that only a very small change in $\lambda(t)$ through a critical value leads to a robust “jump” in the period and so we do not need a large change in anything if the system is near the critical value.

There is still a lot that could be done to improve the model. For the model one should optimize parameter choices by looking for the best fit against climate data. Complementary to this it would be good to analyse the predictability of the times of transitions between the $i/g/G$ states for this model and the locking to astronomical forcing, as well as the influence of initial conditions on the phase of the locking; see e.g. (De Saedeleer et al. 2013). We leave this for future study.

Our current study does not seriously consider the effect of noise on the system due to the fact that good agreement to the climate record can be found just considering the deterministic system with astronomical forcing. However clearly a more sophisticated model must take stochastic perturbations into account. For example, it would be interesting to see if the changes in deterministic and stochastic variance (Meyers and Hinnov 2010) are visible in a noise-forced version of this model as well as to study the effect of

noise on the transitions in the slow-fast system (Berglund and Gentz 2002). Again, we leave this for future study.

Acknowledgments We thank Sebastian Wieczorek, Martin Krupa and Frank Kwasiok for discussions in relation to this work; PA thanks the University of Copenhagen for hospitality and EPSRC via CliMathNet EP/K003216/1 for arranging meetings that facilitated this work, and Martin Rasmussen and Jeroen Lamb for arranging a “Workshop on Critical Transitions in Complex Systems” in 2012 where this was first discussed. We thank the referees and Anna von der Heydt for their insightful comments.

Appendix: The functional form of the slow manifold

We choose the following form for $H(y, v, \lambda)$:

$$H(y, v, \lambda) = h_0 \tanh^{-1}(y) + h_1 y + h_2 v + h_3 + h_4 \frac{(y + h_6)e^{-h_5 v}}{1 + h_7(y + h_8)^2} + \lambda \quad (11)$$

where h_i are all non-negative constants that will be chosen. Setting $h_4 = 0$ and choosing $h_{0,1,2}$ appropriately gives hysteresis between stable sheets of the slow manifold close to $y \approx \pm 1$ for fixed v and varying λ there will be a range of λ with two stable sheets (i and G) while for $\lambda \rightarrow \pm\infty$ there will only be one stable sheet near $y \approx \pm 1$. This can be seen by approximating $\tanh^{-1}(y) = y + y^3/3 + \mathcal{O}(y^5)$, thus for y small $H(y, v, \lambda) = 0$ becomes $(h_0 + h_1)y + h_0 y^3/3 + h_3 + \lambda = h_2 v$. Setting $h_4 > 0$ introduces an additional “cusp” to the slow manifold that gives an extra possible stable value of $-1 < y < 1$ (g) for fixed v (namely three states) and allows us to see transitions between the equilibrium states follow the selection-rules proposed by Paillard. The constants h_i are chosen for (11) as follows:

$$h_0 = 4, \quad h_1 = -6.9, \quad h_2 = -7, \quad h_3 = 2.80847, \quad h_4 = 50, \\ h_5 = 5, \quad h_6 = 0.1, \quad h_7 = 80, \quad h_8 = 0.2. \quad (12)$$

This choice gives a topology for the slow manifold that is robust (small changes in parameters do not change the sheets and the transitions between sheet of the slow manifold). The value of h_3 is chosen so that we have a change in the selection rules as we decrease λ through 0 in (5); more precisely, h_3 is chosen so that there is a critical point $(v, y, \lambda) = (\tilde{v}, \tilde{y}, 0)$ where $H_y = H_v = 0$.

References

- Abe-Ouchi A, Saito F, Kawamura K, Raymo ME, Okuno J, Takahashi K, Blatter H (2013) Insolation-driven 100,000-year glacial cycles and hysteresis of ice-sheet volume. *Nature* 500:190–193
- Ashkenazy Y, Tziperman E (2004) Are the 41 kyr oscillations a linear response to Milankovitch forcing? *Quat Sci Rev* 23:1879–1890
- Benoît E, Callot JL, Diener F, Diener M (1981) Chasse au canards, i–iv. *Collect Math* 32:37–119

- Benzi R, Parisi G, Sutera A, Vulpiani A (1982) Stochastic resonance in climate change. *Tellus* 34:10–16
- Berger A (1978) Long-term variations of daily insolation and quaternary climatic change. *J Atmos Sci* 35:2362–2367
- Berger A (2012) A brief history of the astronomical theories of paleoclimates. In: Berger A, Mesinger F, Sijacki D (eds) *Climate Change*. Springer Vienna, pp 107–129. ISBN:978-3-7091-0972-4
- Berglund N, Gentz B (2002) Metastability in simple climate models: pathwise analysis of slowly driven Langevin equations. *Stoch Dyn* 2:327–356
- Clark PU, Pollard D (1998) Origin of the middle Pleistocene transition by ice sheet erosion of regolith. *Paleoceanography* 13:1–9
- Clark PU, Archer D, Pollard D, Blum JD, Rial JA, Brovkin V, Mix AC, Pisias NG, Roy M (2006) The middle pleistocene transition: characteristics, mechanisms, and implication for long-term changes in atmospheric pCO₂. *Quart Sci Rev* 25:3150–3184
- Crucifix M (2012) Oscillators and relaxation phenomena in Pleistocene climate theory. *Philos Trans R Soc A* 370:1140–1165
- Daruka I, Ditlevsen P (2014) Changing climatic response: a conceptual model for glacial cycles and the mid-Pleistocene transition. *Clim Past Discuss* 10:1101–1127
- De Saedeleer B, Crucifix M, Wiczorek S (2013) Is the astronomical forcing a reliable and unique pacemaker for climate? A conceptual model study. *Clim Dyn* 40:273–294. doi:10.1007/s00382-012-1316-1
- Ditlevsen PD (2009) The bifurcation structure and noise assisted transitions in the Pleistocene glacial cycles. *Paleoceanography* 24:PA3204
- Golombek D, Rosenstein R (2010) Physiology of circadian entrainment. *Physiol Rev* 90:1063–1102
- Golubitsky M, Schaeffer M (1985) Singularities and groups in bifurcation theory, vol 1. Springer, New York
- Hays J, Imbrie J, Shackleton N (1976) Variations in earth's orbit: pacemaker of the ice ages. *Science* 194:1121–1132
- Hilgen FJ, Lourens LJ, van Dam JA (2012) The Neogene period. In: Gradstein F, Ogg J, Schmitz M, Ogg G (eds) *The geological time scale*. Elsevier, Amsterdam, p 923978
- Huybers P (2007) Glacial variability over the last 2 ma: an extended depth-derived age model, continuous obliquity pacing, and the pleistocene progression. *Quat Sci Rev* 26:37–55
- Huybers P (2009) Pleistocene glacial variability as a chaotic response to obliquity forcing. *Clim Past* 5:481488
- Huybers P, Wunsch C (2004) A depth-derived pleistocene age model: Uncertainty estimates, sedimentation variability, and nonlinear climate change. *Paleoceanography* 19:PA1028
- Imbrie J, Imbrie-Moore A, Lisiecki L (2011) A phase-space model for Pleistocene ice volume. *Earth Planet Sci Lett* 307:94–102
- Källén E, Crafoord C, Ghil M (1979) Free oscillations in a climate model with ice-sheet dynamics. *J Atmos Sci* 36:2292–2303
- Krupa M, Szmolyan P (2001) Relaxation oscillation and canard explosion. *J Differ Equ* 174:312–368
- Kuznetsov Y (2004) *Elements of applied bifurcation theory*, 3rd edn. Springer, New York
- Laskar J, Robutel P, Joutel F, Boudin F, Gastineau M, ACM C, Levrard B (2004) A long-term numerical solution for the insolation quantities of the earth. *Astron Astrophys* 428:261285
- LeTreut H, Ghil M (1983) Orbital forcing, climate interactions, and glacial cycles. *J Geophys Res* 88:5167–5190
- Lisiecki LE, Raymo ME (2005) A Pliocene–Pleistocene stack of 57 globally distributed benthic D18O records. *Paleoceanography* 20:PA1003
- Maasch K, Saltzman B (1990) A low-order dynamical model of global climate variability over the full pleistocene. *J Geophys Res* 95:1955–1963
- McClymont E, Sodian S, Rosell-Mele A, Rosenthal Y (2013) Pleistocene sea-surface temperature evolution: early cooling, delayed glacial intensification, and implications for the mid-Pleistocene climate transition. *Earth Sci Rev* 123:173–193
- Meyers SR, Hinno L (2010) Northern hemisphere glaciation and the evolution of Plio-Pleistocene climate noise. *Paleoceanography* 25:PA3207
- Mudelsee M, Schulz M (1997) The mid-Pleistocene climate transition: onset of 100 ka cycle lags ice volume buildup by 280 ka. *Earth Planet Sci Lett* 151:117–123
- North GRIP members (2004) High resolution climate record of the northern hemisphere reaching into the last glacial interglacial period. *Nature* 431:147–151
- Paillard D (1998) The timing of pleistocene glaciations from a simple multiple-state climate model. *Nature* 391:378–381
- Pelletier JD (2003) Coherence resonance and ice ages. *J Geophys Res* 108(D20):4645. doi:10.1029/2002JD003,120
- Rial JA, Oh J, E R (2013) Synchronization of the climate system to eccentricity forcing and the 100,000-year problem. *Nat Geosci* 6:289293
- Saltzman B, Sutera A (1987) The mid-Quaternary climate transition as the free response of a three-variable dynamical model. *J Atmos Sci* 44:236–241
- Shackleton NJ, Hall MA, Vincent E (2000) Phase relationships between millennial-scale events 64,000–24,000 years ago. *Paleoceanography* 15:565–569
- Sima A, Paul A, Schulz M, Oerlemans J (2006) Modeling the oxygen–isotopic composition of the North American ice sheet and its effect on the isotopic composition of the ocean during the last glacial cycle. *Geophys Res Lett* 33(L15):706
- Tziperman E, Gildor H (2003) On the mid-Pleistocene transition to 100-kyr glacial cycles and the asymmetry between glaciation and deglaciation times. *Paleoceanography* 18:1–8
- Wechselberger M (2012) A propos de canards. *Trans AMS* 364:3289–3309